Dynamical behavior of hydrodynamic Lyapunov modes in coupled map lattices

Hong-liu Yang* and Günter Radons†
Institute of Physics, Chemnitz University of Technology, D-09107 Chemnitz, Germany
(Received 12 August 2005; published 12 January 2006)

In our previous study of hydrodynamic Lyapunov modes (HLMs) in coupled map lattices, we found that there are two classes of systems with different λ-k dispersion relations. For coupled circle maps we found the quadratic dispersion relations $\lambda \sim k^2$ and $\lambda \sim k$ for coupled standard maps. Here, we carry out further numerical experiments to investigate the dynamic Lyapunov vector (LV) structure factor which can provide additional information on the Lyapunov vector dynamics. The dynamic LV structure factor of coupled circle maps is found to have a single peak at $\omega=0$ and can be well approximated by a single Lorentzian curve. This implies that the hydrodynamic Lyapunov modes in coupled circle maps are nonpropagating and show only diffusive motion. In contrast, the dynamic LV structure factor of coupled standard maps possesses two visible sharp peaks located symmetrically at $\pm\omega_u$. The spectrum can be well approximated by the superposition of three Lorentzian curves centered at $\omega=0$ and $\pm\omega_u$, respectively. In addition, the ω-k dispersion relation takes the form $\omega_u=c_u k$ for $k \to 2\pi/L$. These facts suggest that the hydrodynamic Lyapunov modes in coupled standard maps are propagating. The HLMs in the two classes of systems are shown to have different dynamical behavior besides their difference in spatial structure. Moreover, our simulations demonstrate that adding damping to coupled standard maps turns the propagating modes into diffusive ones alongside a change of the λ-k dispersion relation from $\lambda \sim k$ to $\lambda \sim k^2$. In cases of weak damping, there is a crossover in the dynamic LV structure factors; i.e., the spectra with smaller k are akin to those of coupled circle maps while the spectra with larger k are similar to those of coupled standard maps.

DOI: 10.1103/PhysRevE.73.016208 PACS number(s): 05.45.Jn, 05.45.Ra, 05.20.−y, 63.10.+a

I. INTRODUCTION

In a recent paper we have reported our results of numerical experiments on hydrodynamic Lyapunov modes (HLMs) in coupled map lattices (CML's) [1]. Here, hydrodynamic Lyapunov modes are the collective tangent-space perturbations associated with the smallest Lyapunov exponents of a high-dimensional dynamical system. They were originally found by Posch and Hirschl in molecular-dynamics simulations of hard-ball systems (see [2]). Due to its potential importance in understanding fundamental problems of statistical mechanics from the point view of nonlinear dynamics [3–8], great interest among many research groups has been triggered by this new finding and a large amount of work has been performed both numerically and analytically in order to gain a deep understanding of the nature of HLMs [9–16]. Numerical simulations were carried out mainly for hard-ball systems in two- and three-dimensional space [2,9,13]. Theoretical attempts to understand the mechanism of HLMs include the random matrix approximation method of Eckmann and Gat [10], the generalized hydrodynamics theory by McNamara and Mareschal [11], and the perturbative analysis in terms of Goldstone modes by de Wijn and van Beijeren [12]. The existence of HLMs in systems with a soft-potential interaction was recently reported for Lennard-Jones and WCA fluids [15,17]. Although lots of work has been performed already, a thorough understanding of this problem has not yet been achieved. Therefore further numerical experiments need to be carried out to accumulate more information on HLMs.

In Ref. [1] we reported results on Lyapunov instabilities of coupled map lattices [18–20]. Although the CMLs under investigation are not directly related to many-particle systems, they do bear similar symmetries, which are believed to be crucial for HLMs. Due to the simplicity of their model dynamics and the ease of numerical simulations, CMLs are ideal for the study of HLMs. Our discovery of HLMs in CMLs suggests that the existence of HLMs is not restricted to many-particle systems and seems to be a common feature of a large class of spatially extended systems. This greatly enlarges the regime where HLMs are expected. Moreover, a Hamiltonian structure is shown not to be a necessary condition for the appearance of HLMs. One important finding is that CMLs belong to two universality classes with respect to the nature of HLMs. The λ-k dispersion relation extracted from static Lyapunov vector (LV) structure factors is characterized by $\lambda \sim k$ for Hamiltonian systems while it takes the form $\lambda \sim k^2$ for dissipative cases. Furthermore, we performed extensive numerical experiments to explore the conditions under which HLMs are expected. The role of conservation laws and symmetries, damping, and on-site potentials was elaborated. The static correlation functions of Lyapunov vectors are the main focus of these studies. Although these quantities are capable of characterizing the spatial structure of LVs quite well and of identifying the existence of HLMs unambiguously, there is a complete lack of information on the dynamical behavior of the modes [16].

In this paper, the recently introduced *dynamic LV structure factor*, which can provide detailed information on the dynamics (especially the coherent movements) of HLMs [16], is adopted to investigate HLMs in CMLs. Our aim is to

*Electronic address: hongliu.yang@physik.tu-chemnitz.de
†Electronic address: radons@physik.tu-chemnitz.de

identify the form of the dynamic LV structure factor and to figure out the difference in LV dynamics between the two classes of systems classified according to the λ-k dispersion relation in our previous study. Additionally, we are interested in seeing how the damping added in a Hamiltonian system influences the LV dynamics, since the asymptotic λ-k dispersion relation for coupled standard maps under damping was found to be akin to that of coupled circle maps.

The rest of this paper is organized in the following way: The model systems under investigation will be given in Sec. II. In Sec. III we will briefly recall the correlation function theory of Lyapunov vectors. In Sec. IV, the intermittent time evolution of the instantaneous static LV structure factors will be demonstrated. Section V is the main part of this paper, in which we will present numerical results for the dynamic LV structure factors of the two models and fit the spectra with properly chosen functions. The fitting parameters obtained will also be analyzed. The effect of damping will also be discussed in this section. Finally, we will list the main results obtained and end this article with a short discussion.

II. MODELS

In this paper, two basic model systems are used to investigate the dynamics of HLMs. The first one is a lattice of standard maps with forcelike coupling [22],

$$v_{t+1}^l = (1-\gamma_t^l)v_t^l + \epsilon[f(u_t^{l+1}-u_t^l) - f(u_t^l - u_t^{l-1})], \quad (1a)$$

$$u_{t+1}^l = u_t^l + v_{t+1}^l, \quad (1b)$$

where $f(z)=(1/2\pi)\sin(2\pi z)$, t is the index of the time step, $l=\{1,2,\ldots,L\}$ is the index of lattice site, and L is the system size. The second model is a lattice of circle maps with forcelike coupling,

$$u_{t+1}^l = u_t^l + \epsilon[f(u_t^{l+1}-u_t^l) - f(u_t^l - u_t^{l-1})]. \quad (2)$$

Here, $f(z)=(1/2\pi)\sin(2\pi z)$ and t, l, and L have the same meaning as in Eq. (1).

We set $\gamma_t^l=0$ for the time being and use periodic boundary conditions unless otherwise stated.

Note that the quantities $P=\Sigma_l v_t^l$ for coupled standard maps, Eqs. (1), and $Q=\Sigma_l u_t^l$ for coupled circle maps, Eq. (2), are conserved during iterations of the system dynamics and both systems are invariant with respect to an arbitrary translation in the u direction.

An essential difference between the two systems is that the model of coupled standard maps is a Hamiltonian system preserving the phase volume while coupled circle maps are dissipative with the phase volume contracting constantly as time proceeds. Our previous results indicated that the two systems belong to different universality classes with respect to the λ-k dispersion relation of HLMs [1]. Now, we will turn to the dynamical behavior of HLMs in the two systems.

III. CORRELATION FUNCTIONS OF LYAPUNOV VECTORS

In order to facilitate the reading of this paper, we briefly repeat the correlation function theory of Lyapunov vectors in this section. Details can be found in [15,16].

In the spirit of the correlation function theory in molecular hydrodynamics [21], we define a dynamical variable named LV fluctuation density as

$$\mathcal{U}^{(\alpha)}(r,t) = \sum_{l=1}^{L} \delta u_t^{(\alpha)l}\delta(r-r_l), \quad (3)$$

where $r_l \equiv la$ is the position coordinate of the lth element of CML's and $\{\delta u_t^{(\alpha)l}\}$ is the u part of the αth Lyapunov vector. A space- and time-dependent autocorrelation of LV fluctuation density is defined as

$$G_u^{(\alpha\alpha)}(r,t) = \langle \mathcal{U}^{(\alpha)}(r,t)\mathcal{U}^{(\alpha)}(0,0)\rangle, \quad (4)$$

where $\langle\cdots\rangle$ means the time and ensemble average. The so-called static LV structure factor is the Fourier transformation of the equal-time correlation function $G_u^{(\alpha\alpha)}(r,0)$,

$$\begin{aligned} S_u^{(\alpha\alpha)}(k) &= \int G_u^{(\alpha\alpha)}(r,0)e^{-ikr}\mathrm{d}r \\ &= \sum_{l=1}^{N} G_u^{(\alpha\alpha)}(la,0)e^{-ikla} \\ &= \langle \mathcal{U}_k^{(\alpha)}(t)\mathcal{U}_{-k}^{(\alpha)}(t)\rangle \\ &= \langle s_u^{(\alpha\alpha)}(k,t)\rangle, \end{aligned} \quad (5)$$

with

$$\mathcal{U}_k^{(\alpha)}(t) = \int \mathcal{U}^{(\alpha)}(r,t)e^{-ikr}\mathrm{d}r = \sum_{l=1}^{L}\delta u_t^{(\alpha)l}e^{-ikr_l} \quad (6)$$

being the spatial Fourier transformation of $\mathcal{U}^{(\alpha)}(r,t)$ and

$$s_u^{(\alpha\alpha)}(k,t) = \mathcal{U}_k^{(\alpha)}(t)\mathcal{U}_{-k}^{(\alpha)}(t) \quad (7)$$

being the instantaneous static LV structure factor. From Eq. (5) we learn that the static LV structure factor is nothing but the spatial power spectrum of the LV fluctuation density $\mathcal{U}^{(\alpha)}(r,t)$. In Eq. (7), we introduce an instantaneous quantity $s_u^{(\alpha\alpha)}(k,t)$, which will be used alongside the dynamic structure factor to study the LV dynamics.

Note that the spatial Fourier transformation is taken with regard to the discrete lattice space, not the state space of CML's.

The dynamic LV structure factor is defined as

$$\begin{aligned} S_u^{(\alpha\alpha)}(k,\omega) &= \int \mathrm{d}t e^{i\omega t}\int G_u^{(\alpha\alpha)}(r,t)e^{ikr}\mathrm{d}r \\ &= \int \langle \mathcal{U}_k^{(\alpha)}(t)\mathcal{U}_{-k}^{(\alpha)}(0)\rangle e^{i\omega t}\mathrm{d}t, \end{aligned} \quad (8)$$

which contains detailed information on the LV dynamics.

For the simplicity of calculations, we take the lattice constant $a=1$ throughout the rest of the paper.

IV. INTERMITTENCY IN THE TIME EVOLUTION OF LYAPUNOV VECTORS

In this section, we consider the time evolution of the instantaneous quantity $s_u^{(\alpha\alpha)}(k,t)$, which is the spatial power

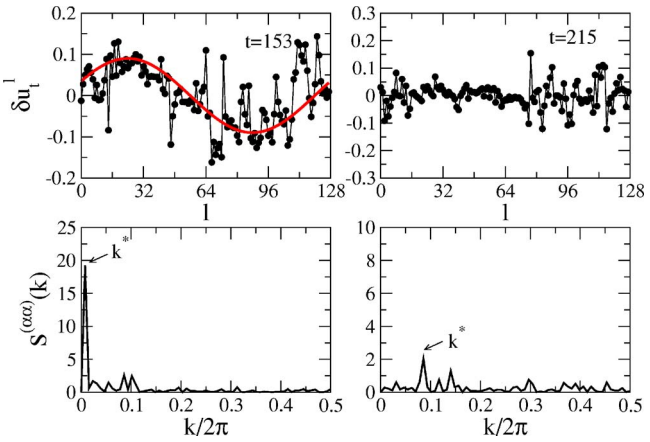

FIG. 1. (Color online) Two snapshots of the instantaneous profile of LV No. 116 (upper row) and the corresponding spatial power spectra $s_u^{(\alpha\alpha)}(k,t)$ (lower row) for coupled standard maps with $\epsilon=1.3$. The system size $L=128$ is set for all figures concerning the coupled standard maps unless otherwise stated.

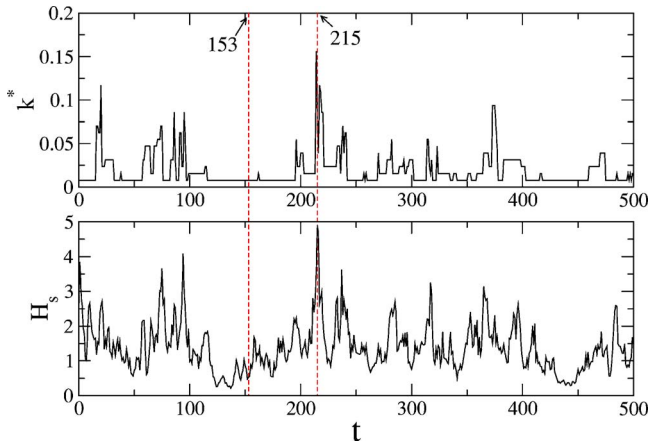

FIG. 2. (Color online) Intermittent time evolution of the peak wave number k^* (upper panel) and the spectral entropy $H_s(t)$ (lower panel) of coupled standard maps with $\epsilon=1.3$.

spectrum of LV fluctuation density at the moment t. We will first demonstrate what happens in coupled standard maps before we turn to coupled circle maps.

A. Coupled standard maps

In Fig. 1, two typical snapshots of the profile $\mathcal{U}^{(\alpha)}(r,t)$ and the corresponding spatial power spectra $s_u^{(\alpha\alpha)}(k,t)$ for Lyapunov vector No. 116 of coupled standard maps are presented. Note that, for the used system size $L=128$, there exist $2L=256$ Lyapunov vectors and that, due to the standard ordering, LV No. 116 lies near the center of the Lyapunov spectrum–i.e., in a regime where hydrodynamic Lyapunov modes exist [1]. The LV profile at $t=153$ is roughly a plane wave, and there is a sharp peak in its spatial power spectrum $s_u^{(\alpha\alpha)}(k,t)$. The wave number k^* of the sharp peak is comparable with $2\pi/L$, the smallest nontrivial wave number permitted by the periodic boundary conditions used. In contrast, the LV profile at $t=215$ is rather noisy and no long-wavelength structure is visible. The corresponding spatial Fourier spectrum is nearly uniform, and there is no sharp peak as in the case $t=153$. From these results we see that the time evolution of Lyapunov vectors is not stationary and the structure of Lyapunov vectors varies erratically with time. The investigations mentioned above also show that the instantaneous quantity $s_u^{(\alpha\alpha)}(k)$ is quite sensitive to the structural changes of LVs and is a suitable measure for the characterization of such changes.

For a qualitative characterization of the changes in $s_u^{(\alpha\alpha)}(k,t)$, we employ the quantity called spectral entropy [23], which reads

$$H_s(t) = -\int s_u^{(\alpha\alpha)}(k,t)\ln[s_u^{(\alpha\alpha)}(k,t)]\mathrm{d}k. \tag{9}$$

The time evolution of the wave number k^* and the spectral entropy $H_s(t)$ is shown in Fig. 2. Here, k^* is defined as the wave number where the measure $s_u^{(\alpha\alpha)}(k,t)$ attains its maximal value. The intermittent behavior of both quantities demonstrates clearly that the time evolution of Lyapunov vectors in coupled standard maps, Eq. (1), is not stationary. The dynamic LV structure factor may be used to further clarify whether this is due to a coherent movement or random fluctuations.

B. Coupled circle maps

Snapshots of typical profiles of LV No. 156 of coupled circle maps are shown in Fig. 3. The time evolution of the peak wave number k^* and the spectral entropy $H_s(t)$ is presented in Fig. 4, where similar intermittent behavior as in coupled standard maps is observed. These facts indicate that the LV dynamics of coupled circle maps, Eq. (2), is also nonstationary.

V. DYNAMIC LV STRUCTURE FACTORS

In this section, we will consider the dynamic LV structure factor of the two CMLs. The use of this quantity enables us

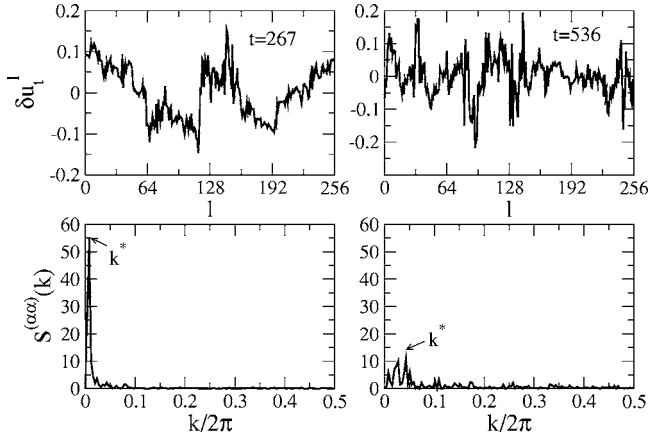

FIG. 3. Two snapshots of the instantaneous profile of LV No. 156 (upper row) and the corresponding spatial power spectra $s_u^{(\alpha\alpha)}(k,t)$ (lower row) for coupled circle maps, Eq. (2), with $\epsilon=1.3$. The system size $L=256$ is set for all figures concerning the coupled circle maps unless otherwise stated. The zero-value Lyapunov exponent is at $\alpha=164$.

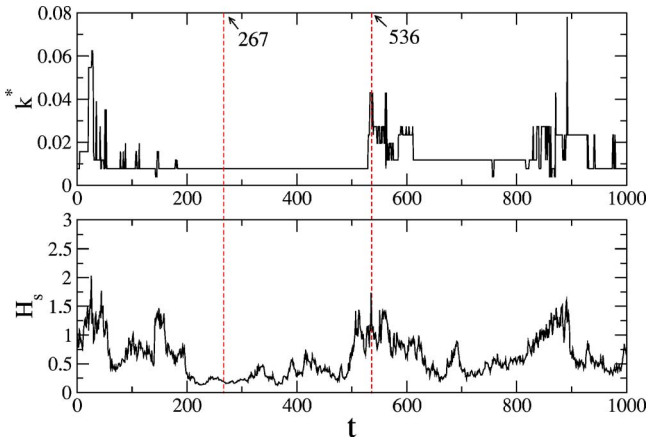

FIG. 4. (Color online) Intermittent time evolution of the peak wave number k^* (upper panel) and the spectral entropy $H_s(t)$ (lower panel) of coupled circle maps, Eq. (2), with $\epsilon=1.3$.

to detect possible coherent movements of HLMs and to clarify the origin of the intermittency observed in Sec. IV. In addition, the information about the form of dynamic LV structure factors gained through numerical experiments may serve as a basis for a future theoretical understanding of the underlying mechanism.

A. Coupled circle maps

The dynamic LV structure factors $S_u^{(\alpha\alpha)}(k,\omega)$ of LV No. 163 of coupled circle maps, Eq. (2), are presented in Fig. 5. All the curves shown with various wave numbers share a common feature: namely, the existence of a peak at $\omega=0$. In addition, no other peaks are visible beside the one just mentioned. The peak is rather significant for $k \gtrapprox 2\pi/L$. As the wave number increases, so does the width of the peak while the hight decreases gradually.

In Fig. 6, the dynamic LV structure factors $S_u^{(\alpha\alpha)}(k,\omega)$ are approximated with the Lorentzian spectrum:

$$S_u^{(\alpha\alpha)}(k,\omega) = a_0 \frac{a_1}{\omega^2 + a_1^2}, \tag{10}$$

where the fitting parameters a_0 and a_1 are generally functions of the wave number k and may also have dependence on

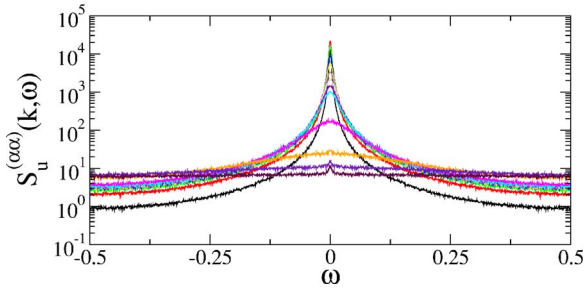

FIG. 5. (Color online) Dynamic LV structure factors $S_u^{(\alpha\alpha)}(k,\omega)$ of LV No. 163 of coupled circle maps, Eq. (2), with $\epsilon=1.3$. The peak at $\omega=0$ becomes weaker as the wave number k increases.

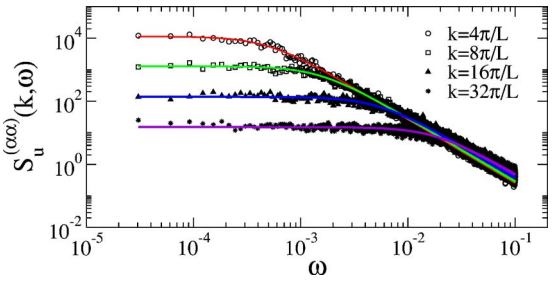

FIG. 6. (Color online) Approximations of the dynamic LV structure factors $S_u^{(\alpha\alpha)}(k,\omega)$ with the Lorentzian curve [see Eq. (10)]. Here the results of LV No. 163 of coupled circle maps are shown with a representation of only the positive ω part of $S_u^{(\alpha\alpha)}(k,\omega)$.

Lyapunov vectors. In the figure one can see that the numerical data agree quite well with the curves from Eq. (10).

In Fig. 7, the variation of the fitting parameter a_1 with changing wave number k is shown. Here, parameters for several cases with different LVs and coupling strengths ϵ are plotted together in the same figure. The gradual ascent of a_0 with k is found to be parabolic—i.e., $a_1 \simeq c_1 k^2$. The values of a_1 have almost no dependence on Lyapunov vectors while the variation of the coupling strength ϵ does lead to a change in a_1. However, the parabolic dependence of a_1 on k is a common feature of all cases investigated. Remember that the λ-k dispersion relation of coupled circle maps is characterized by $\lambda \sim k^2$ [1]. It is not clear whether the identical k dependence is a coincidence or implies some deep connection between them.

In Fig. 8, values of the fitting parameter a_0 are plotted with the wave number k. The corresponding static LV structure factors $S_u^{(\alpha\alpha)}(k)$ are represented in the same figure. For the three example cases with $\alpha=163$, 162, and 159, respectively, there is an excellent agreement between the curves of $S_u^{(\alpha\alpha)}(k)/\pi$ and the symbols for a_0—i.e., $a_0=(1/\pi)S_u^{(\alpha\alpha)}(k)$. Actually, this is what one expects from the general relation $S_u^{(\alpha\alpha)}(k)=\int d\omega S_u^{(\alpha\alpha)}(k,\omega)$ and a dependence as in Eq. (10). The perfect agreement shown in Fig. 8 demonstrates that the Lorentzian approximation in Eq. (10) works quite well for the dynamic LV structure factors of coupled circle maps.

Based on our studies of the fitting parameters, we come to the conclusion that the dynamic LV structure factor $S_u^{(\alpha\alpha)}(k,\omega)$ of coupled circle maps takes the form

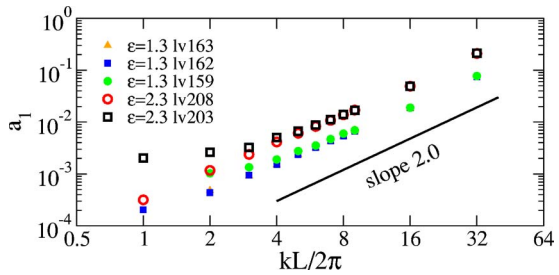

FIG. 7. (Color online) The fitting parameter a_1 vs the wave number k for several cases with various ϵ and α. A straight line with the slope 2.0 is plotted to show the parabolic dependence of a_1 on k.

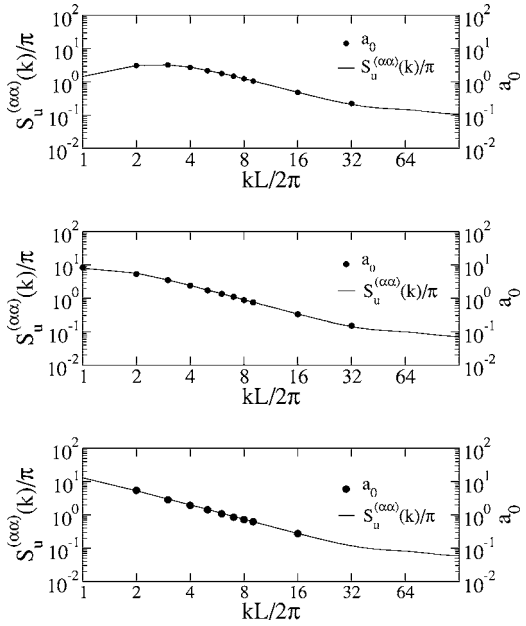

FIG. 8. k dependence of the fitting parameter a_0 of the LV Nos. 159, 162, and 163 (from top to bottom) of coupled circle maps with $\epsilon=1.3$. The corresponding static structure factors are shown in the same plot, respectively. The agreement between curves and symbols implies a linear relation $a_0 \simeq (1/\pi) S_u^{(\alpha\alpha)}(k)$.

$$S_u^{(\alpha\alpha)}(k,\omega) = \frac{1}{\pi} S_u^{(\alpha\alpha)}(k) \frac{c_1 k^2}{\omega^2 + c_1^2 k^4}, \tag{11}$$

where $S_u^{(\alpha\alpha)}(k)$ is the static LV structure factor and c_1 is a k-independent constant.

Equation (11) represents a single Lorentzian spectrum centered at $\omega=0$, with the half-height width $2c_1k^2$. A spectrum of this form is typical of a diffusive process in $\mathcal{U}^{(\alpha)}(r,t)$ described by the equation

$$\frac{d\mathcal{U}^{(\alpha)}(r,t)}{dt} = D\nabla_r^2 \mathcal{U}^{(\alpha)}(r,t), \tag{12}$$

where ∇_r means the spatial derivative with regard to the discrete lattice space and the diffusion constant $D=c_1$.

Now it becomes clear that the intermittency shown in Fig. 4 is a result of the diffusive motion of LVs.

B. Coupled standard maps

We will now turn to coupled standard maps. Figure 9 shows the dynamic LV structure factors $S_u^{(\alpha\alpha)}(k,\omega)$ of LV No. 126. In contrast to coupled circle maps, the spectrum $S_u^{(\alpha\alpha)}(k,\omega)$ possesses two sharp peaks at $\omega=\pm\omega_u$, respectively. With the wave number k increasing, the two peaks tend to separate further; i.e., ω_u becomes larger. At the same time, the peak widths broaden and the peak heights decrease. The dynamic LV structure factors $S_v^{(\alpha\alpha)}(k,\omega)$ for the v component of the same LV are presented in the lower panel of Fig. 9. They are similar to $S_u^{(\alpha\alpha)}(k,\omega)$.

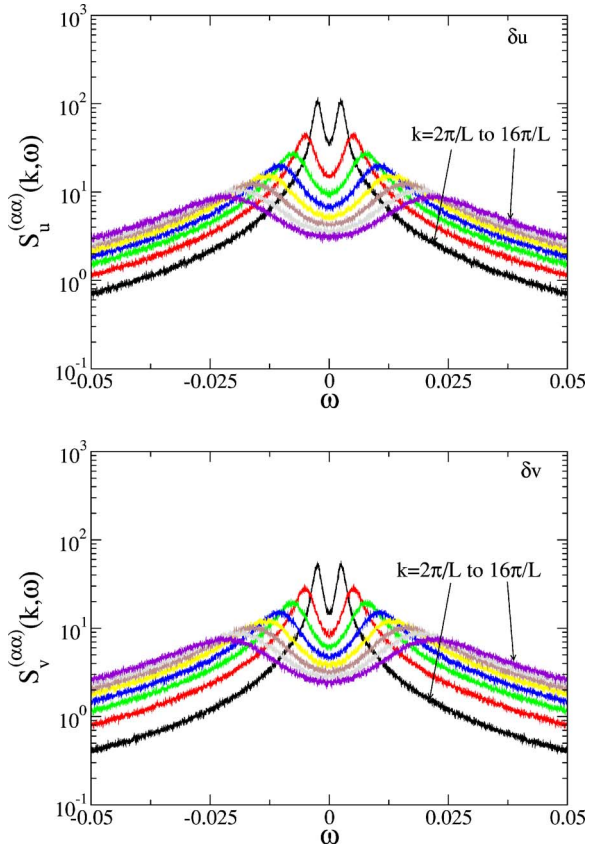

FIG. 9. (Color online) Dynamic LV structure factors of LV No. 126 of coupled standard maps with $\epsilon=0.6$. The upper panel shows those for the u component of LVs and the lower panel depicts those for the v component. A distinct feature of the spectra is the existence of two sharp peaks centering symmetrically at $\omega=\pm\omega_u$.

In Fig. 10, numerical data of $S_u^{(\alpha\alpha)}(k,\omega)$ are approximated with the superposition of three Lorentzian spectra centered at $\omega=0$ and $\pm\omega_u$, respectively—i.e. with

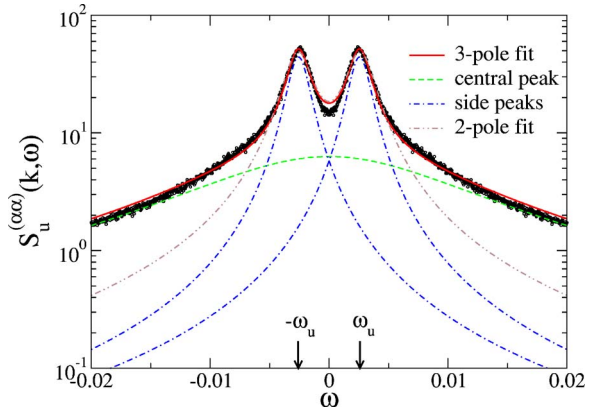

FIG. 10. (Color online) three- and two-pole approximations of the dynamic LV structure factor $S_u^{(\alpha\alpha)}(k,\omega)$ of LV No. 126 of coupled standard maps with $\epsilon=0.6$ and $k=2\pi/L$. Obviously the three-pole fit is better than the two-pole fit although the central peak of the three-pole fit is quite weak and flat.

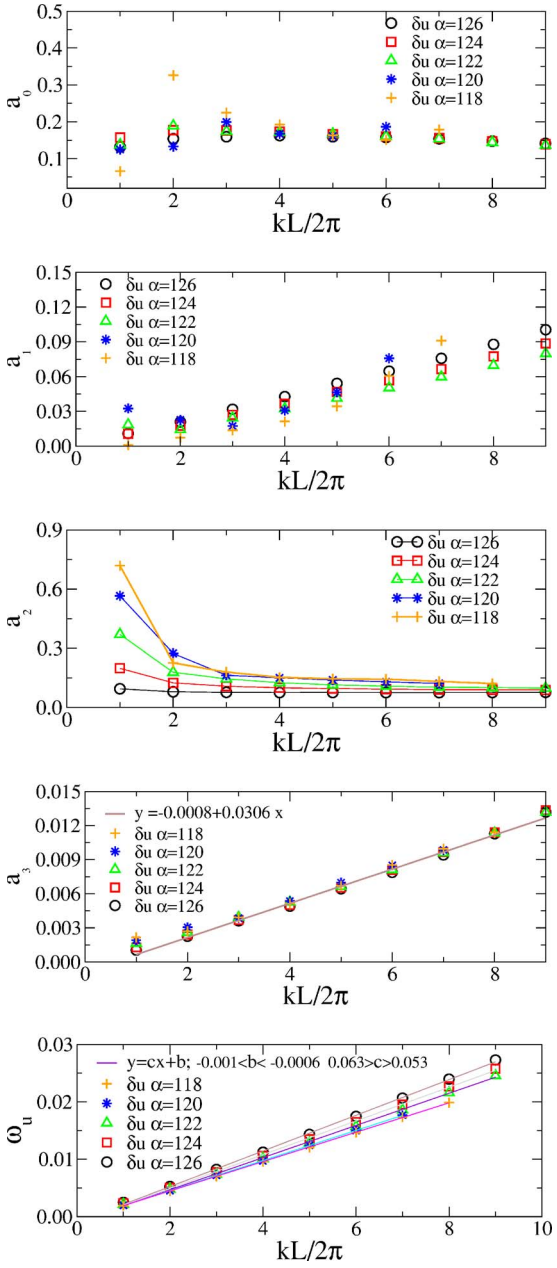

FIG. 11. (Color online) The fitting parameters of the three-pole approximations of dynamic structure factors of five LVs of coupled standard maps with $\epsilon=0.6$.

$$S_u^{(\alpha\alpha)}(k,\omega) = a_0\frac{a_1}{\omega^2+a_1^2} + a_2\frac{a_3}{(\omega+\omega_u)^2+a_3^2} + a_2\frac{a_3}{(\omega-\omega_u)^2+a_3^2}, \tag{13}$$

where the fitting parameters a_i and ω_u may have dependence on the wave number k and the LV being used. From Fig. 10 one can see that the three-pole approximation works fairly well. The estimated central peak at $\omega=0$ is quite flat compared to the two side peaks at $\omega=\pm\omega_u$. We have tried to fit the data with a two-pole spectrum without the central peak. As shown in the figure, the result is much worse than the three-pole fitting, especially for the large-ω regime. Therefore, the three-pole approximation for the dynamic LV structure factors $S_u^{(\alpha\alpha)}(k,\omega)$ is more suitable than the two-pole fitting, although there are only two visible peaks in the spectra.

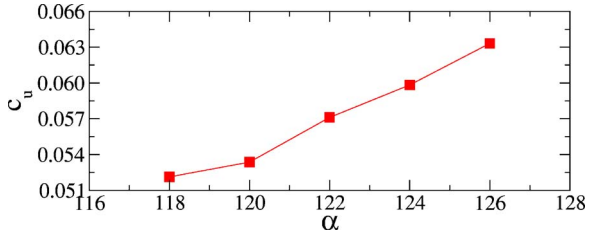

FIG. 12. (Color online) The velocity c_u vs the index α of LVs. The slow increase of c_u with α from 118 to 126 reflects the weak dependence of c_u on LVs.

The k dependences of the fitting parameters taken from the three-pole approximations of five LVs of coupled standard maps with $\epsilon=0.6$ are presented in Fig. 11. Remember that since the estimated central peak at $\omega=0$ is rather weak, the fitting parameters a_0 and a_1 are less accurate and less reliable than the parameters of the side peaks. Below, we will explore the fitting parameters one by one.

We will begin with a_3 which is the half-height width of the side peaks. The collapse of data for different LVs on a single curve implies that this quantity does not depend on LVs, or at least the dependence is too weak to be detected. The ascent of a_3 with increasing k can be well approximated with a linear function $a_3 \simeq c_3 k$ with $c_3=0.0306$.

The finite widths of the side peaks mean that the coherent motion represented by these peaks is of finite lifetime. The k dependence of a_3 reflects that each of the Fourier components has its own lifetime.

The value of ω_u increases gradually with raising k. The scattering of data especially for the large-k regime implies the dependence of ω_u on LVs. Numerical fitting of data to a linear function $\omega_u=\omega_{u0}+c_u k$ yields $-0.001<\omega_{u0}<-0.0006$ and $0.053<c_u<0.063$. To further investigate the dependence of the velocitylike quantity c_u on LVs, it is plotted against α in Fig. 12. As can be seen, the dependence is rather weak.

The existence of shifting side peaks in the spectra $S_u^{(\alpha\alpha)}(k,\omega)$ implies that the LVs of coupled standard maps possess some coherent movements. In other words, the HLMs in this system are propagating.

In Fig. 13, some profiles of the dynamic LV structure factors $S_u^{(\alpha\alpha)}(k,\omega)$ of LV No. 163 with wave numbers k larger than those shown in Fig. 9 are presented. Although there are still two visible peaks in each spectrum, as in the cases with lower wave numbers, we failed to approximate them well with the three-pole spectrum of Eq. (13). The dependence of ω_u on k is represented in the lower panel of Fig. 13. With increasing k, the curve deviates gradually from the linear relation $\omega_u=c_u k$, which fits the data in the regime $k\approx 0$ quite well. And the curve levels off eventually at $k\approx 120\pi/L$. Since it is impossible to perform the three-pole fitting for the large-k cases, positions of the maximum in the spectra are used instead.

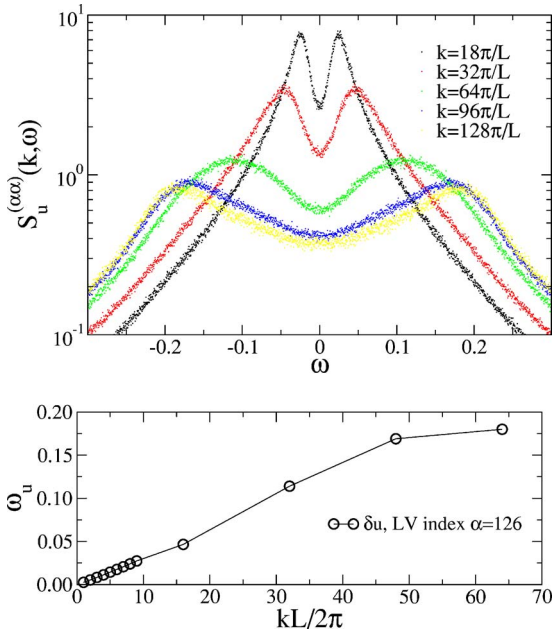

FIG. 13. (Color online) Dynamic LV structure factors $S_u^{(\alpha\alpha)} \times(k,\omega)$ of LV No. 126 with several larger wave numbers k (upper panel) and the k dependence of ω_u (lower panel). The different meanings of ω_u for larger and smaller k are described in the main text.

The k dependence of a_2, the weight of the side peak, is shown in Fig. 11. It reminds us of the static LV structure factors of the corresponding LVs. In Fig. 14 the plots of a_2 are overlaid with those of the static LV structure factors $S_u^{(\alpha\alpha)}(k)$. For the case $\alpha=122$, the symbols for a_2 follow the curve of the static LV structure factor quite closely. This agreement gives the relation $a_2=c_2 S_u^{(\alpha\alpha)}(k)$ with $c_2=0.375\pi$.

Motivated by the intuitive expectation that the central peak here should represent the same dynamics as in coupled circle maps, it is natural to anticipate a linear relation between a_0 and the static LV structure factor. Therefore, we plot a_0 together with a_2 in Fig. 14. For the case $\alpha=122$, a_0 is larger than a_2 but follows the general trend of a_2 for $k \geqslant 4\pi/L$. For $k=2\pi/L$ and $4\pi/L$, the side peaks at $\omega = \pm\omega_u$ are so sharp that they prevent an accurate estimation of the parameters a_0 and a_1 for the central peak. If we ignore the part with $k \leqslant 4\pi/L$, it is reasonable to say that $a_0 = c_0 S_u^{(\alpha\alpha)}(k)$ with a constant c_0 different from c_2. The situation is more evident for the case $\alpha=118$ where we assign $a_0=a_2$ for the numerical fitting and the estimated parameters show confidently that $a_0=a_2=c_2 S_u^{(\alpha\alpha)}(k)$ with $c_2=\pi/3$. These numerical experiments suggest a plausible conjecture that both a_0 and a_2 are proportional to the static LV structure factor $S_u^{(\alpha\alpha)}(k)$. The ratio of the two prefactors c_0 and c_2, however, depends on the LVs used. In Fig. 15, the ratio a_2/a_0 is plotted with k for three LVs. Obviously, for each LV the ratio is nearly constant for $k \geqslant 6\pi/L$ and it takes different values for different LVs. This result is consistent with our above conjecture.

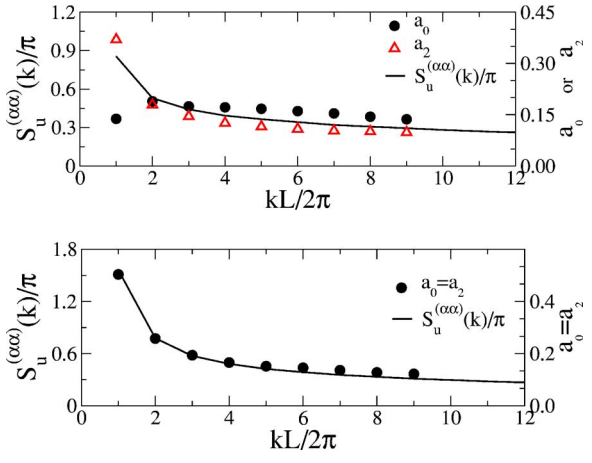

FIG. 14. (Color online) k dependence of the fitting parameters a_2 and a_0 and the static LV structure factors $S_u^{(\alpha\alpha)}(k)$ of the LV No. 122 (upper panel) and No. 118 (lower panel) of coupled standard maps with $\epsilon=0.6$. In case $\alpha=118$ we assign $a_0=a_2$ for the three-pole approximation.

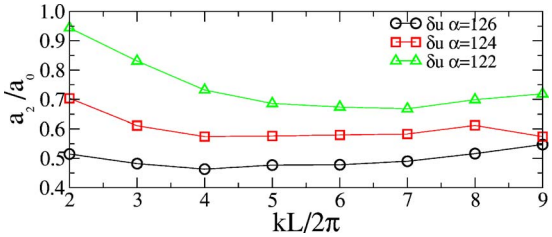

FIG. 15. (Color online) Ratio a_2/a_0 vs k of the LV Nos. 122, 124, and 126 of coupled standard maps with $\epsilon=0.6$. It is nearly constant for $k \geqslant 6\pi/L$ but hold different values for various LVs.

The width a_1 of the central peak shown in Fig. 11 is much broader than a_3, the width of side peaks. This means the central peak is much flatter than the side peaks. Data of a_1 are also more noisy and have much stronger dependence on α than a_3. In spite of this, the values of a_1 for all LVs considered show the general tendency to ascend with increasing k. To make the k dependence more obvious, in Fig. 16 we show the log-log plot of a_1 against k. For the same reason stated above, the values of a_1 with $k=2\pi/L$ are ignored. The scattering of data is more obvious than in the linear plot. Numerical fitting of the data to a power-law function $a_1 = c_1 k^{\beta}$ yields $\beta \simeq 1.0$.

After performing individual investigations of each fitting parameter, we will now attempt to bring all components together and arrive at the estimated form of the dynamic LV structure factor of coupled standard maps. It reads

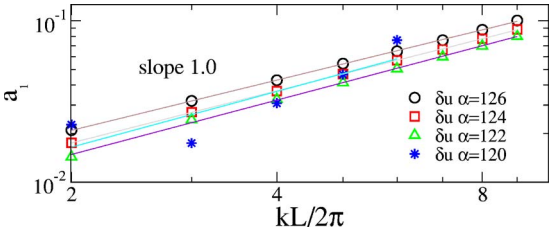

FIG. 16. (Color online) Log-log plot of the fitting parameter a_1 of coupled standard maps with $\epsilon=0.6$. Numerical fitting of the data to a power-law function $a_1 \sim k^{-\beta}$ yields $\beta \simeq 1.0$.

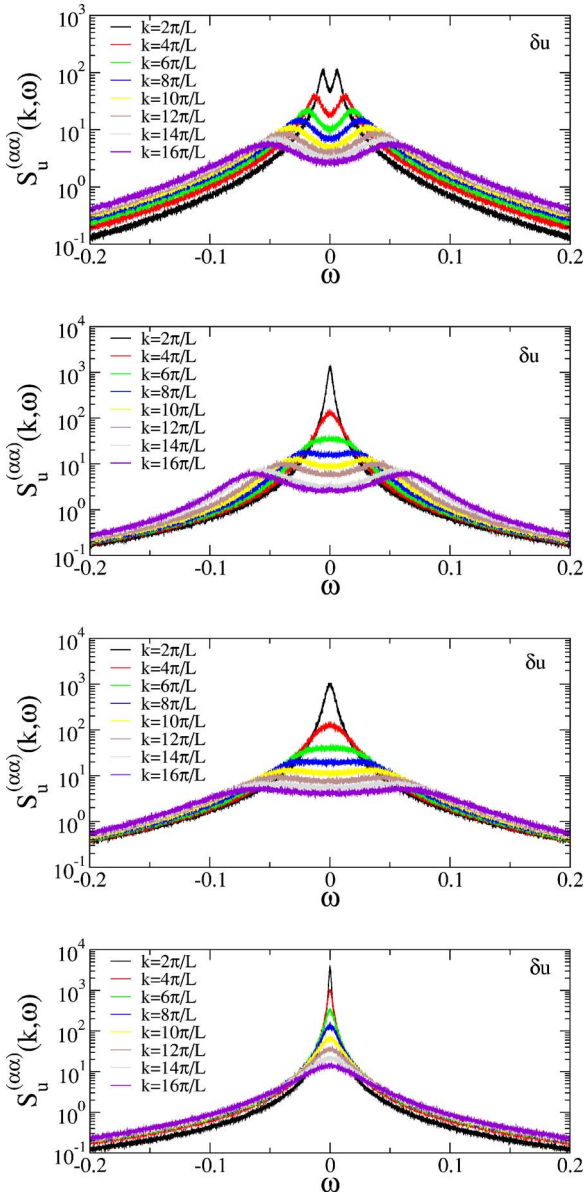

FIG. 17. (Color online) Dynamic LV structure factors $S_u^{(\alpha\alpha)}(k,\omega)$ of coupled damped standard maps under damping. The damping coefficient is $\gamma_0=0.0$, 0.2, 0.5, and 0.7 (from top to bottom), respectively. The coupling strength is $\epsilon=1.3$. The side peaks in the spectra fade out gradually with increasing γ_0.

$$S_u^{(\alpha\alpha)}(k,\omega) = S_u^{(\alpha\alpha)}(k)\left[c_0\frac{c_1k^\beta}{\omega^2+c_1^2k^{2\beta}} + c_2\frac{c_3k}{(\omega+\omega_u)^2+c_3^2k^2} + c_2\frac{c_3k}{(\omega-\omega_u)^2+c_3^2k^2}\right], \quad (14)$$

where c_i are k-independent constants and $S_u^{(\alpha\alpha)}(k,\omega)$ is the static LV structure factor. In particular, c_1 and c_3 are independent of the LVs being used while the ratio c_2/c_0 does change with α. The spectrum, Eq. (14), is akin to that of density fluctuations in fluids [21]. It consists of three components: the central peak at $\omega=0$ and two side peaks at $\omega=\pm c_uk$. The two shifting side peaks correspond to the phononlike propagating mode while the central peak represents the decaying diffusive mode. The finite width of the side peaks implies that the propagating mode is of finite lifetime similar to phononlike modes in fluids. The diffusive mode corresponds to anomalous diffusion of the LVs.

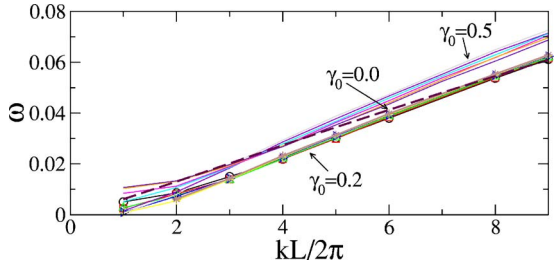

FIG. 18. (Color online) The fitting parameter ω_u vs k for the three cases $\gamma_0=0.0$, 0.2, and 0.5. Fitting data to a linear function $\omega_u=c_uk$ gives $c_u=0.136$, 0.161, and 0.175, respectively.

Simulations for other cases with the coupling strengths $\epsilon=1.3$ and 2.3 give similar results to those shown above. The value of c_u depends on the coupling strength ϵ.

C. Effect of damping on the dynamics of HLMs

In our previous study [1], we found that adding damping to coupled standard maps induces the change of the λ-k dispersion relation from $\lambda\sim k$ to $\lambda\sim k^2$. In cases of weak damping, a crossover in the dispersion relation may be observed; i.e., the dispersion relation turns from $\lambda\sim k$ in the large-k regime into the asymptotic form $\lambda\sim k^2$ with decreasing k. In this section we will look at the corresponding change in the dynamical behavior of the HLMs. For simplicity, we restrict the discussion to $\gamma_t'=\gamma_0$.

In Fig. 17 the dynamic LV structure factors $S_u^{(\alpha\alpha)}(k,\omega)$ of coupled standard maps under damping are presented [see Eq. (1)]. Four cases with increasing damping strength are arranged together to make the change more evident. As the damping strength increases, the general trend of variation in $S_u^{(\alpha\alpha)}(k,\omega)$ is that the side peaks fade out gradually. Close investigation detects that the change in the spectra begins with those that have small wave numbers. For the case $\gamma_0=0.2$ (the second panel from the top in Fig. 17), the side peaks in the spectra with $k\leqslant 6\pi/L$ already become invisible while those in the spectra with $k\geqslant 10\pi/L$ are still rather sharp. This is assumed to correspond to the previously observed crossover in the λ-k dispersion relation.

For the case $\gamma_0=0.7$, all spectra possess only the central peak, just like the spectra for coupled circle maps (see Fig. 5). These results show that in connection with the change in λ-k dispersion relation, the propagating HLMs in coupled standard maps become diffusive under damping. Although the HLMs with wavelengths comparable to the system size become diffusive, the modes with $k\gg 2\pi/L$ are still propagating if the damping is not too strong. The situation is similar to the existence of shear waves in fluids on the mesoscopic scale [21].

In the recent study of many-particle systems with hard-core interaction, de Wijn and von Beijeren [12] pointed out that there is a certain relation between the propagating HLMs

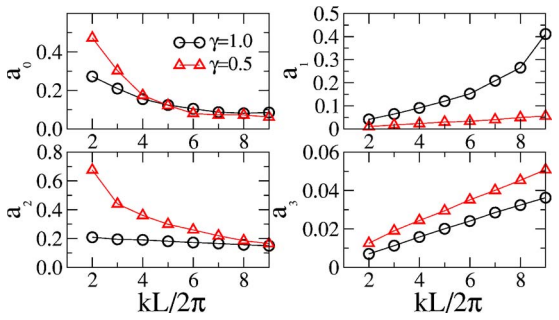

FIG. 19. (Color online) The fitting parameters a_i for the dynamic LV structure factors of coupled damped standard maps with $\gamma=1.0$ and 0.5.

and the imaginary eigenvalues of the fundamental matrix governing the time evolution of the perturbations in tangent space. One ingredient essential for such an interpretation is the time translational invariance possessed by many-particle systems. The absence of such a continuous symmetry in the CML's under consideration calls for an alternative interpretation of the propagating modes observed.

To specify the changes in the spectra, we will try to fit the spectra with the three-pole formula in Eq. (13), as in the case without damping. Since only the central peak is visible in the spectra with small wave numbers, one should keep in mind that the fitting parameters obtained for the cases with large k are more accurate and more reliable than those for small k. In Fig. 18, the fitting parameter ω_u is plotted against k for three cases with different damping coefficients γ_0. All of them can be well fitted with a linear function $\omega_u=c_u k$. Here, c_u

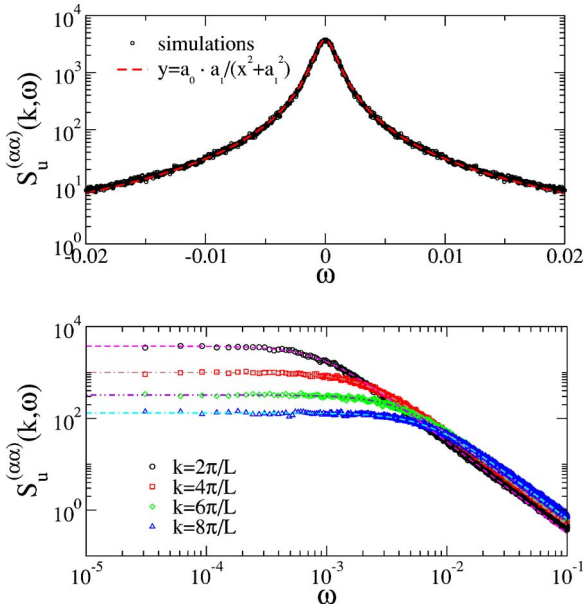

FIG. 20. (Color online) Approximation of the spectrum $S_u^{(\alpha\alpha)}(k,\omega)$ of LV No. 76 of the overdamped case $\gamma_0=0.7$. The upper panel is the log-linear plot for the case $k=2\pi/L$, and the lower panel is the log-log plot for four cases with $k=2\pi/L$ to $8\pi/L$. The agreement between the numerical data and the fitting curves is perfect for all cases shown. The zero-value Lyapunov exponent is at $\alpha=78$.

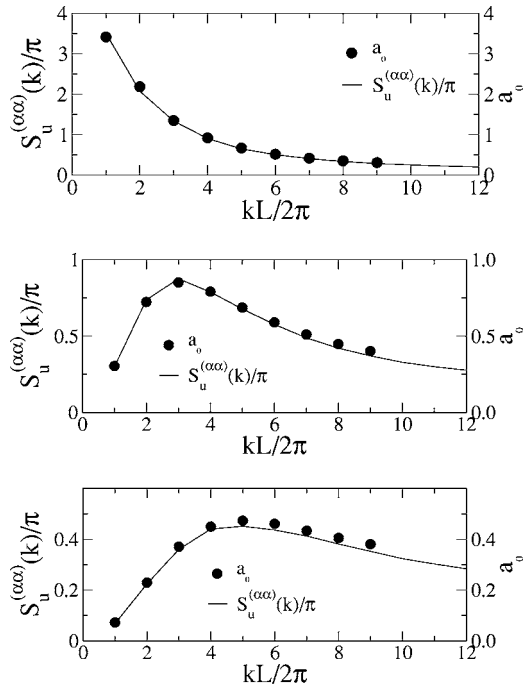

FIG. 21. k dependence of the fitting parameter a_0 and the corresponding static LV structure factors $S_u^{(\alpha\alpha)}(k)$ of the LV Nos. 76, 72, and 68, respectively (from top to bottom). The agreement between the two sets yields $a_0=(1/2\pi)S_u^{(\alpha\alpha)}(k)$.

$=0.136$, 0.161, and 0.175 for $\gamma_0=0.0$, 0.2, and 0.5, respectively. The slight increase in the velocity c_u may be the result of the inaccurate estimations of ω_u. Figure 19 shows the change in the fitting parameters a_i.

We will now turn to the overdamped case with $\gamma_0=0.7$ (see the bottom panel of Fig. 17). In Fig. 20, the dynamic structure factor of LV No. 76 with $k=2\pi/L$ is approximated with a single Lorentzian curve as stated in Eq. (10). Obviously, there is a perfect agreement between the numerical data and the fitting curve. The lower panel of Fig. 20 shows that the approximation works well for all cases with different k values that has been considered.

The fitting parameter a_0 and the corresponding static LV structure factors are plotted in Fig. 21. There is a rather good agreement between the symbols for a_0 and the curves of the spectra $S_u^{(\alpha\alpha)}(k)$. This implies the relation $a_0=(1/\pi)S_u^{(\alpha\alpha)}(k)$, similar to the one we found for coupled circle maps.

In Fig. 22, the width a_1 of the peaks in the spectra $S_u^{(\alpha\alpha)}(k,\omega)$ is plotted against the wave number k. It increases with k for all the cases investigated. Numerical fitting of the data of LV No. 76 to a power-law function $a_1 \sim k^\beta$ yields $\beta \simeq 2.0$. With decreasing α from 76, which corresponds to increasing the Lyapunov exponent $\lambda^{(\alpha)}$ from zero, the curves bend up on the small-k side. Nevertheless, they tend to follow the parabolic function $a_1 \sim k^2$ for large wave numbers. Thus, we can say that the dynamic LV structure factors of the overdamped case with $\gamma_0=0.7$ take the form shown in Eq. (11) for coupled circle maps. The same interpretation as for coupled circle maps can be adopted here as well; i.e., the diffusive motion of the LVs leads to the estimated Lorentzian spectrum $S_u^{(\alpha\alpha)}(k,\omega)$.

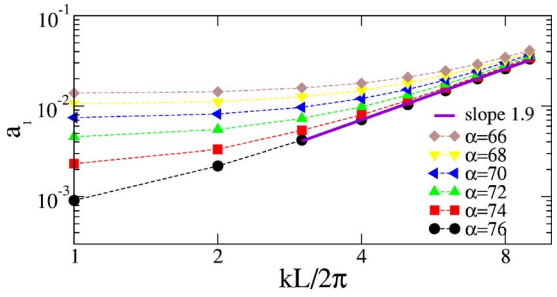

FIG. 22. (Color online) The width a_1 of the peak in the spectra $S_u^{(\alpha\alpha)}(k,\omega)$ vs k for various LVs. Numerical fitting of the data for the case $\alpha=76$ gives $a_1 \sim k^2$. Curves for other LVs follow the same trend for large k, although they depart from the parabolic function $a_1 \sim k^2$ in the small-k regime.

VI. VISUALIZING THE LV DYNAMICS

In the above sections, we showed that there are differences in the dynamic LV structure factors of the coupled Hamiltonian and dissipative maps. In this section, we would like to use particular examples to visualize the LV dynamics of the two kinds of systems and to demonstrate the differences between them. This will also be helpful in understanding the physical meaning of the peaks in the dynamic LV structure factors.

To this aim, we set

$$f(z) = \begin{cases} z/r & \text{for } 0 \leqslant z < r, \\ (1-z)/(1-r) & \text{for } r \leqslant z < r, \end{cases} \tag{15}$$

in Eqs. (1) and (2), instead of the nonlinear function $f(z) = (1/2\pi)\sin(2\pi z)$ used above. Here, $r \in [0,1)$ is a control parameter which can be used to tune the tangent-space dynamics of the coupled maps. For example, for $\epsilon > 0$, decreasing r causes the systems, Eqs. (1) and (2), to become more hyperbolic. As shown in Fig. 23, for the dissipative system, Eq. (2), with $\epsilon=1.3$ and $r=0.2$, each of the static LV structure factors is highly dominated by a Fourier component with wave number k_{max}. The corresponding Lyapunov vector is nearly a pure plane wave. With increasing r, the dominant peaks in the static LV structure factors become broader and the LV profile departs from the shape of a pure plane wave. A similar scenario is observed for the Hamiltonian case, Eq. (1).

An animation of the time evolution of the LV No. 254 of the model, Eq. (2), for the piecewise linear f of Eq. (15) can be found on the web site http://www.tu-chemnitz.de/ksnd/hya/hlm-cml. The system size $L=256$, the coupling strength $\epsilon=1.3$ and $r=0.2$.

In Fig. 24, the time evolution of the quantity $s_u^{(\alpha\alpha)}(k_{max},t)$ is presented, where $s_u^{(\alpha\alpha)}(k,t)$ is the instantaneous static LV structure factor defined in Eq. (7) and k_{max} is the wave number of the dominant peak in the static LV structure factor $S_u^{(\alpha\alpha)}(k)$. The time evolution is characterized by the sequence of erratic events. In between the events, $s_u^{(\alpha\alpha)}(k_{max},t)$ maintains a nearly constant value $L/2$. As shown in Fig. 25, which is the enlargement of the event at $t \approx 7720$, at the beginning of each event the value of

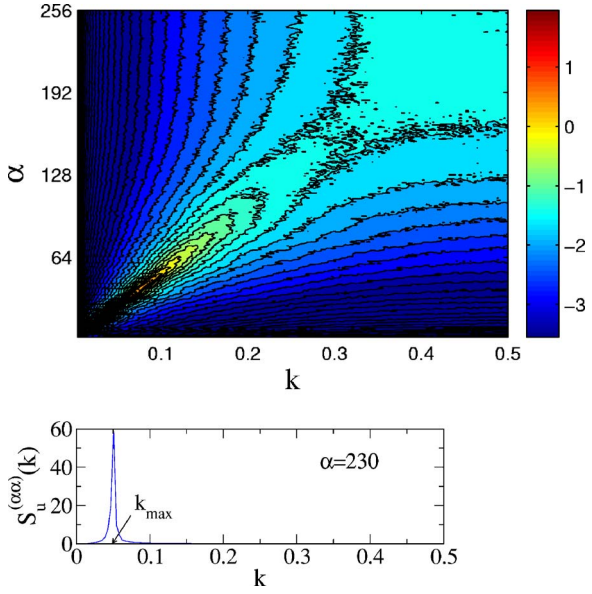

FIG. 23. (Color online) The upper panel shows the contour plot of the static LV structure factors of the dissipative system, Eq. (2), with the nonlinear function $f(z)$ in Eq. (15). Here, $\epsilon=1.3$ and $r=0.2$. The lower panel displays the static LV structure factor of LV No. 230. The dominant peak is very sharp here, which implies that the LV profile is rather close to a pure plane wave.

$s_u^{(\alpha\alpha)}(k_{max},t)$ suddenly dips downward; then, it relaxes gradually to the constant value $L/2$. Several snapshots of the LV profile $\mathcal{U}^{(\alpha)}(r,t)$ during this event are shown in Fig. 25. Obviously, the dip of $s_u^{(\alpha\alpha)}(k_{max},t)$ at the beginning of the event is triggered by the deformation of the LV profile from a pure plane wave. The decay of the deformation corresponds to the slow relaxation process following the sudden dip. As shown in Fig. 25, a numerical fit of the relaxation of the quantity $s_u^{(\alpha\alpha)}(k_{max},t)$ to an exponential function works rather well, which implies that the decay of the deformation in $\mathcal{U}^{(\alpha)}(r,t)$ is exponential. This is consistent with the argument given in Sec. V A about the dynamic LV structure factors. In other words, the diffusivelike exponential decay of the defor-

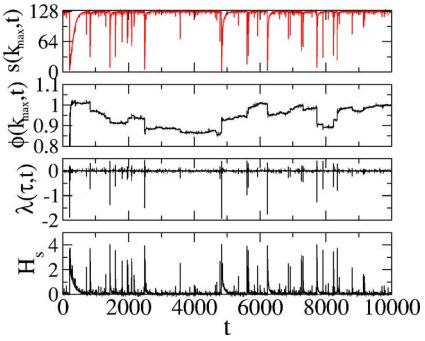

FIG. 24. (Color online) Time evolution of several quantities characterizing the LV dynamics. The erratic dip-relaxation events in $s_u^{(\alpha\alpha)}(k_{max},t)$ are a manifestation of the diffusive motion of $\mathcal{U}^{(\alpha)}(r,t)$. The phase $\phi(k_{max},t)$ is nearly constant during the intervals between the dip-relaxation events. This implies that the LVs are of nonpropagating nature in this system.

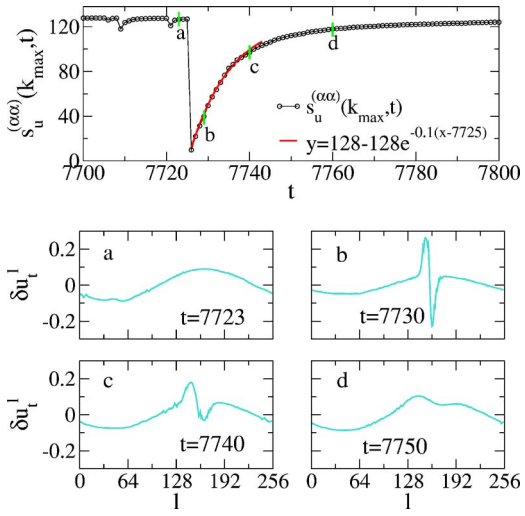

FIG. 25. (Color online) The upper panel shows the dip-relaxation event in $s_u^{(\alpha\alpha)}(k_{max},t)$ at $t\approx 7720$. Four snapshots of the LV profile $\mathcal{U}^{(\alpha)}(r,t)$ during this dip-relaxation event are represented in the lower panels. It becomes clear from the plot that the dip-relaxation event is characterized by the sudden deformation and slow recovering of the plane-wave LV profile.

mation in $\mathcal{U}^{(\alpha)}(r,t)$ gives rise to the Lorentzian spectrum shape of the dynamic LV structure factor.

The time evolution of the quantity $\phi(k_{max},t)$ is also shown in Fig. 24. Here, $\phi(k,t)$ is defined as the phase variable of the quantity $\mathcal{U}_k^{(\alpha)}(t)$ given in Eq. (6). In the cases studied in this section, the LV profile $\mathcal{U}^{(\alpha)}(r,t)$ comes close to a pure plane wave most of the time. Thus, the quantity $\phi(k_{max},t)$ is a suitable measure to characterize the movement of LVs. As can be seen in Fig. 24, the phase variable $\phi(k_{max},t)$ remains constant within the range of error during the long quiet intervals between the dip-relaxation events in $s_u^{(\alpha\alpha)}(k_{max},t)$. It suddenly jumps as the dips in $s_u^{(\alpha\alpha)}(k_{max},t)$ take place. This demonstrates clearly that, here, the Lyapunov vector shows no movement apart from the irregular dip-relaxation events. Note that it is nonpropagating in nature.

Figure 24 also shows the finite-time Lyapunov exponent $\lambda(\tau,t)$ with $\tau=1$. It is well known that Lyapunov exponents (LEs) characterize the chaoticity of nonlinear systems in certain directions in phase space. In general, the degree of chaoticity of nonlinear dynamical systems fluctuates with time. To characterize such nonuniform nature, a quantity named finite-time or local Lyapunov exponent is introduced. It is defined as the average expanding exponent of the trajectory segment from t to $t+\tau$. See Ref. [24] for a rigorous definition of this quantity. The time evolution of $\lambda(\tau,t)$ shown here is characterized by a series of spikelike sudden jumps. Note that the spikelike fluctuations take place simultaneously with the dip-relaxation events in $s_u^{(\alpha\alpha)}(k_{max},t)$. This indicates an interesting connection between them.

The spectral entropy $H_s(t)$ defined in Eq. (9) is represented in the bottom panel of Fig. 24. The figure indicates that the intermittency discussed in Sec. IV is a manifestation of the observed structural changes in the LVs.

In Fig. 26, the time evolutions of quantities $s_u^{(\alpha\alpha)}(k_{max},t)$ and $\lambda(\tau,t)$ for several LVs are shown together. The connection between the changes in the two quantities is quite obvious. For instance, at $t\approx 108$ there are sudden dips in $s_u^{(\alpha\alpha)}(k_{max},t)$ for LVs with $\alpha=252$ and 253. Correspondingly, there are spikelike strong fluctuations in the finite-time LE's with $\alpha=252$ and 253 at the right moment. At $t\approx 204$ and 385, the pair of LVs involved are $\alpha=\{251,254\}$ and $\{252, 253\}$, respectively. At $t\approx 726$ and 837, four s are all involved in the dip-relaxation event. These facts encourage the conjecture that the intermittent time evolution of the LV profile is due to the interaction of a group of LVs.

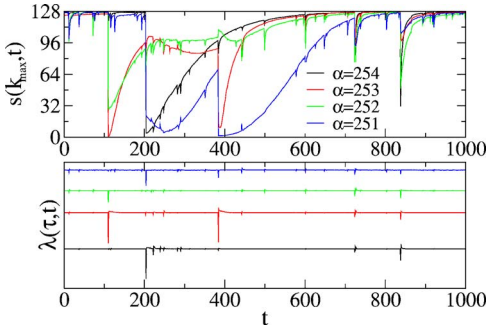

FIG. 26. (Color online) The coherence between the dip-relaxation events in the time evolution of $s_u^{(\alpha\alpha)}(k_{max},t)$ and the spikelike fluctuations in $\lambda(\tau,t)$ for several LVs shows that the dip-relaxation events are caused by the interaction among LVs.

An animation of the time evolution of LV No. 126 of the model, Eq. (1), can also be found on the web site http://www.tu-chemnitz.de/ksnd/hya/hlm-cml. Here, the system size $L=128$, the coupling strength $\epsilon=1.3$, and $r=0.15$.

In Fig. 27, the time evolution of the same quantities as discussed above is presented for the Hamiltonian system, Eq. (1), with $f(z)$ from Eq. (15). Similar to the dissipative system, Eq. (2), the time evolution of $s_u^{(\alpha\alpha)}(k_{max},t)$ is characterized by a series of dip-relaxation events. In connection with such events, there are sudden jumps in the values of the phase variable $\phi(k_{max},t)$ and strong spikelike fluctuations in the finite-time Lyapunov exponents $\lambda(\tau,t)$. As shown in Fig. 28, the dip-relaxation events here also represent the same

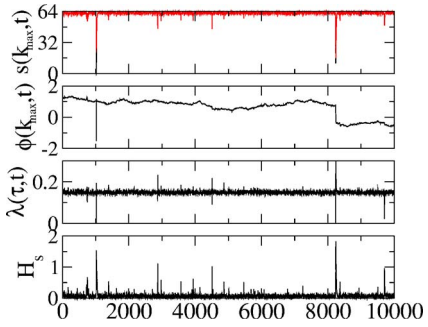

FIG. 27. (Color online) Same as Fig. 24, but for the Hamiltonian system, Eq. (1). Here, $\epsilon=1.3$ and $r=0.15$. The dip-relaxation events are similar to those in Fig. 24. Note that, in contrast to the dissipative case shown in Fig. 24, the phase $\phi(k_{max},t)$ changes continuously during the intervals between dip-relaxation events. This implies that the LVs in this system are propagating. The apparent stochastic motion of the phase variable $\phi(k_{max},t)$ means that the propagating Lyapunov modes are of short lifetime.

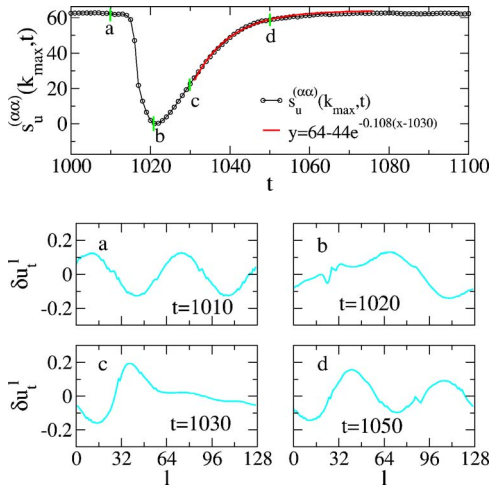

FIG. 28. (Color online) The upper panel shows the enlargement of the dip-relaxation event at $t \approx 1010$. Four snapshots of the LV profile $\mathcal{U}^{(\alpha)}(r,t)$ during this dip-relaxation event are presented in the lower panels. As can be clearly seen from the plot, the dip-relaxation event resembles those in the dissipative case; i.e., they are characterized by the sudden deformation and slow recovering of the plane-wave LV profile.

geometrical changes in the LV profile. This supports our conjecture that the central peak in the dynamic LV structure of the Hamiltonian system has a similar physical meaning as the peak in the dynamic LV structure of the dissipative system.

In contrast to the dissipative case, the phase variable $\phi(k_{max},t)$ varies continuously during the quiet intervals between the dip-relaxation events. Such continuous changes in the phase variable $\phi(k_{max},t)$ become more evident in the case $\epsilon=1.3$ and $r=0.1$ (cf. Fig. 29). In that case, the sudden jumps that are due to the dip-relaxation events disappear completely for the time period shown. The phase variable $\phi(k_{max},t)$, however, evolves continuously as time goes on. The continuous variation of the phase variable implies that the Lyapunov vectors in this system propagate along the lattice space. The stochastic evolution of $\phi(k_{max},t)$ means that the direction of propagation changes frequently; i.e., the propagating modes in this case are of finite lifetime. The propagation of the LVs gives rise to the side peaks in the dynamic LV structure factors.

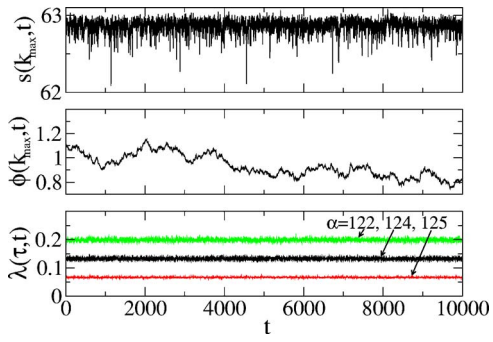

FIG. 29. (Color online) Same as Fig. 27, but for the case $\epsilon=1.3$ and $r=0.1$. Here, the wild dip-relaxation events disappear completely, which causes the continuous variation of the phase variable $\phi(k_{max},t)$ to become more evident. Note that the fluctuations of the finite-time Lyapunov exponents are very small compared to the differences between neighboring Lyapunov exponents. This is the reason why the dip-relaxation events disappear here.

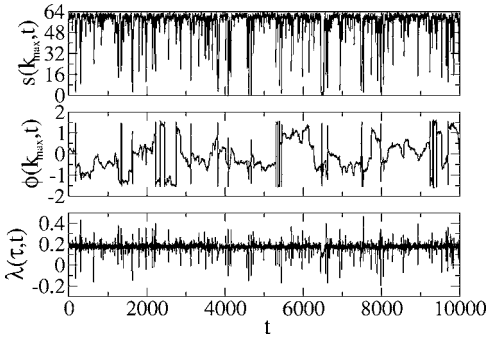

FIG. 30. Same as Fig. 27, but for the case $\epsilon=1.3$ and $r=0.2$. Here, the dip-relaxation events become more frequent in comparison with the case $\epsilon=1.3$ and $r=0.15$. Note that the sudden jump in the phase variable $\phi(k_{max},t)$ and the spikelike fluctuations in $\lambda(\tau,t)$ also take place more frequently.

In a general extended dynamical system with continuous symmetries, the LVs associated with near-zero LEs are of long-wavelength structure. The LV profiles are, however, rather far from the shape of a pure plane wave. Therefore, the visualization of the LV dynamics as shown above becomes difficult. A similar mechanism as discussed earlier, however, is expected to work in general. In other words, the deformation and relaxation of the LV profile give rise to the central peak in the dynamic LV structure factors. The side peaks in the dynamic LV structure factors represent the propagation of the LVs. As shown in Fig. 30, for the case $r=0.2$ the dip-relaxation events become more frequent compared to the case $r=0.15$ (cf. Fig. 27). As r further increases, the dip-relaxation events become so frequent that one can no longer distinguish individual events. This is the general case for a nonhyperbolic system.

VII. CONCLUSION AND DISCUSSION

In summary, we have investigated numerically the dynamical behavior of Lyapunov vectors in coupled map lattices. We found that the dynamic LV structure factors of coupled circle maps have a single peak at $\omega=0$, while two sharp peaks centered at $\pm\omega_u$ are visible in the dynamic LV structure factors of coupled standard maps. The dynamic LV structure factors of coupled circle maps take the form of a single Lorentzian spectrum which is typical of a diffusive process. This implies that the hydrodynamic Lyapunov modes in coupled circle maps show only diffusive motion and are nonpropagating. The spectra of coupled standard maps can be well approximated by a superposition of three Lorentzian peaks centered at $\omega=0$ and $\pm\omega_u$, respectively. The shifting side-peaks represent the propagating hydrodynamic Lyapunov modes while the central peak comes from the diffusive motion of LVs. The difference found here supports our conjecture that the two models belong to different universal-

ity classes. We have also studied the effect of damping added to coupled standard maps and found that the side peaks in dynamic LV structure factors fade out gradually with increasing damping strength. This is connected with the crossover in the λ-k dispersion relation discovered in our previous study [1].

In both models, the peaks in the spectra (either the central peaks or the side peaks) are of finite width. This means that the modes represented by these peaks have finite lifetimes. The intermittency discussed in Sec. IV is an indication of the finite lifetime of the modes. It is, however, difficult to extract a precise time scale from the intermittent time series and to compare it with the time scale derived from the peak width. The reason for this difficulty lies in the fact that the intermittent time evolution of each Lyapunov vector is the combined effect of many Fourier components with different wave numbers, each of which has its own lifetime.

We have shown that there are differences between the HLMs of coupled standard maps and those of coupled circle maps, both in the spatial structure and in the dynamical behavior. Further investigations of numerous systems, including the dynamical *XY* model and the Kuramoto-Sivashinsky equation, support our conjecture that there are two classes of systems with difference in the nature of HLMs. More details of this will be presented elsewhere.

In many-particle systems, three different kinds of HLMs have been proposed [14]. The transverse modes are stationary. The longitudinal and *P* modes are coupled together, and both are propagating. In a two-dimensional system, all three modes can be present. In a one-dimensional system, however, the transverse modes are not permitted. In this case, the nonpropagating HLMs found in the one-dimensional lattice of coupled circle maps are unexpected, since only the propagating longitudinal modes, and possibly *P* modes for systems with continuous-time translational invariance, are expected in a one-dimensional system. The existence of propagating HLMs in the one-dimensional lattice of coupled standard maps calls for an alternative explanation to that of the many-particle case. The reason is that, due to the discrete time evolutions of the CMLs the *P* modes are absent here. Thus, the LP pairs formed by the longitudinal and *P* modes can not exist here [14]. The seemingly strange behavior of the HLMs found in this study may be due to the following difference between many-particle systems and coupled map lattices. The elements of coupled map lattices are embedded in a discrete lattice space (the coordinate space) while the time evolutions happen in a continuous state space; i.e., the coordinate and state space are different. In many-particle systems, however, the movement of particles is in the same space where they are located. Further work is needed to clarify this point.

For both systems investigated, the position and width of the peaks in dynamic LV structure factors show only a weak dependence on the LVs. This suggests the interpretation that the Fourier modes indexed by wave number have weakly coupled dynamics and are the fundamental building blocks of the LV dynamics. The interaction of these modes leads to the diffusive motion of the HLMs and the intermittency in the LV time evolutions.

ACKNOWLEDGMENT

We acknowledge financial support from the DFG within SFB393 "Parallele Numerische Simulation für Physik und Kontinuumsmechanik."

[1] H. L. Yang and G. Radons, Phys. Rev. E **73**, 016202 (2005).
[2] H. A. Posch and R. Hirschl, in *Hard Ball Systems and the Lorentz Gas*, edited by D. Szàsz (Springer, Berlin, 2000), p. 279.
[3] N. S. Krylov, *Works on the Foundations of Statistical Mechanics* (Princeton University Press, Princeton, 1979).
[4] P. Gaspard, *Chaos, Scattering, and Statistical Mechanics* (Cambridge University Press, Cambridge, England, 1998).
[5] J. P. Dorfman, *An Introduction to Chaos in Nonequilibrium Statistical Mechanics* (Cambridge University Press, Cambridge, England, 1999).
[6] D. J. Evans and G. P. Morriss, *Statistical Mechanics of Nonequilibrium Liquids* (Academic, New York, 1990).
[7] W. G. Hoover, *Computational Statistical Mechanics* (Elsevier, New York, 1991).
[8] W. G. Hoover, *Time Reversibility, Computer Simulation, and Chaos* (World Scientific, Singapore, 1999).
[9] C. Forster, R. Hirschl, H. A. Posch, and Wm. G. Hoover, Physica D **187**, 294 (2004).
[10] J.-P. Eckmann and O. Gat, J. Stat. Phys. **98**, 775 (2000).
[11] S. McNamara and M. Mareschal, Phys. Rev. E **64**, 051103 (2001); M. Mareschal and S. McNamara, Physica D **187**, 311 (2004).
[12] A. S. de Wijn and H. van Beijeren, Phys. Rev. E **70**, 016207 (2004).
[13] T. Taniguchi and G. P. Morriss, Phys. Rev. E **65**, 056202 (2002); **68**, 026218 (2003); Phys. Rev. Lett. **94**, 154101 (2005).
[14] J.-P. Eckmann, C. Forster, H. A. Posch, and E. Zabey, J. Stat. Phys. **118**, 813 (2005).
[15] H. L. Yang and G. Radons, Phys. Rev. E **71**, 036211 (2005).
[16] G. Radons and H. L. Yang (unpublished).
[17] C. Forster and H. A. Posch, New J. Phys. **7**, 32 (2005).
[18] K. Kaneko, Prog. Theor. Phys. **72**, 480 (1984); K. Kaneko, in *Formation, Dynamics, and Statistics of Patterns*, edited by K. Kawasaki, A. Onuki, and M. Suzuki (World Scientific, Singapore, 1990), Vol. 1.
[19] See the special issue on coupled map lattices in Chaos **2**, 279 (1992).
[20] R. Tenny, L. S. Tsimring, L. Larson, and H. D. I. Abarbanel, Phys. Rev. Lett. **90**, 047903 (2003); T. Bohr, M. van Hecke, R. Mikkelsen, and M. Ipsen, *ibid.* **86**, 5482 (2001); F. Ginelli, R. Livi, A. Politi, and A. Torcini, Phys. Rev. E **67**, 046217 (2003); O. Rudzick and A. Pikovsky, *ibid.* **54**, 5107 (1996); H. L. Yang and E. J. Ding, *ibid.* **50**, R3295 (1994).
[21] J. P. Boon and S. Yip, *Molecular Hydrodynamics* (McGraw-

Hill, New York, 1980).
[22] K. Kaneko and T. Konishi, Phys. Rev. A **40**, 6130 (1989).
[23] R. Livi, M. Pettini, S. Ruffo, M. Sparpaglione, and A. Vulpiani, Phys. Rev. A **31**, 1039 (1985).
[24] H. Fujisaka, Prog. Theor. Phys. **70**, 1264 (1983); R. Benzi, G. Paladin, G. Parisi, and A. Vulpiani, J. Phys. A **18**, 2157 (1985); P. Grassberger, R. Badii, and A. Politi, J. Stat. Phys. **51**, 135 (1988).